Resonance enhanced electron impact excitation for P-like Cu XV*

Li Shuang(李 双)[a)b)], Yan Jun(颜 君)[c)d)], Li Chuan-Ying(李传莹)[c)],
Huang Min(黄 敏)[a)b)], and Chen Chong-Yang(陈重阳)[a)b)†]

[a)] *Applied Ion Beam Physics Laboratory, Fudan University, Shanghai* 200433, *China*
[b)] *Shanghai EBIT Lab, Institute of Modern Physics, Department of Nuclear Science and Technology, Fudan University, Shanghai* 200433, *China*
[c)] *Institute of Applied Physics and Computational Mathematics, Beijing* 100088, *China*
[d)] *Center for Applied Physics and Technology, Peking University, Beijing* 100871, *China*

(Received 21 May 2015; revised manuscript received 30 June 2015; published online 12 October 2015)

Employing both the Dirac $\boldsymbol{R}$-matrix and the relativistic distorted wave with independent process and isolated resonance approaches, we report resonance enhanced electron impact excitation data (specifically, effective collision strengths) among the lowest 41 levels from the $n = 3$ configurations of Cu XV. The results show that the latter approach can obtain resonance contributions reasonably well for most excitations of Cu XV, though a comparison between the two approaches shows that the close-coupling effects are truly significant for rather weak excitations, especially for two-electron excitations from the $3s3p^4$ to $3s^23p^23d$ configuration. Resonance contributions are significant (more than two orders of magnitude) for many excitations and dramatically influence the line intensity ratios associated with density diagnostics.

Keywords: electron impact excitation, resonance excitation, collision strength, Dirac $\boldsymbol{R}$-matrix theory

PACS: 34.50.Fa, 34.80.Dp **DOI:** 10.1088/1674-1056/24/11/113401

1. Introduction

In astrophysical and laboratory plasmas, the spectra (or emission lines) of highly charged P-like ions are often observed.[1] The lines are very helpful in comprehension of density fluctuations and basic processes in both astrophysical and laboratory plasma.[2] Over the decades, many of P-like lines of Cu XV have also been observed in tokamak discharges, laser-produced plasma, or the beam-foil spectrum.[3] Copper and gold can form an alloy, which can be easily used in a Hohlraum (or cavity) as wall material[4] to maximize the laser to x-ray conversion efficiency in inertial confinement fusion (ICF).[5] In addition, the current design of the ignition target in the National Ignition Facility is a capsule of copper-doped beryllium with a smooth deuterium-tritium solid layer on the inner surface.[6] Hence, the emission lines from highly charged ions of copper, including Cu XV, are expected to be of diagnostic potential in the ICF plasma. To achieve this diagnostic goal, it is required that a large number of atomic parameters, such as the rates of electron impact excitation (EIE, which is the current research focus[7–9]). One has to heavily rely on theoretical calculations due to the scarcity of the experimental data.

No reports are available in the literature on the EIE of Cu XV to the best of our knowledge, though a few studies on energy levels and radiative rates are found.[10–12] Previous researches on EIE for other P-like ions, such as S II,[13] Cl III,[14] K V,[15] Ca VI,[16] and Fe XII[2,17–20] showed that resonance contributions can be significant for the EIE data (specifically, effective collision strengths, i.e., Υ values). We note that the $\boldsymbol{R}$-matrix method within a close-coupling framework is adopted for the calculations on the EIE of all these $Z \leq 26$ ions, though they can be treated in a second way, which is based on the first-order Born approximation, as done in the study on direct excitation (DE) in Ni XIV by Landi *et al.*,[21] and the further work performed by Wang *et al.*,[22] in which resonance contributions were included via the independent process and isolated resonance approximation using distorted-waves (hereafter IPIRDW)[23] and the Dirac $\boldsymbol{R}$-matrix (DRM) approach.[24,25] It is found that resonance contributions are also of vital importance for Ni XIV.[22]

In this work, we report on the EIE cross sections among the 41 levels from the $n = 3$ ($3s^23p^3$, $3s3p^4$, and $3s^23p^23d$) configurations of Cu XV. The EIE cross sections and effective collision strengths among these levels are very helpful for density diagnostics.[2,20,21,26] To take into account resonance contributions as in Ref. [22] and assess the accuracy of atomic data, we study the EIE processes by employing both the DRM and the relativistic distorted-wave (RDW) together with the IPIRDW approaches. Both approaches have been integrated in the FAC.[27,28] We deliberately keep target expansion identical for the two approaches. Therefore, the differences between the two approaches are mainly due to the close-coupling ef-

*Project supported by the National Natural Science Foundation of China (Grant Nos. 11076009 and 11374062), the Chinese Association of Atomic and Molecular Data, the Chinese National Fusion Project for ITER (Grant No. 2015GB117000), and the Leading Academic Discipline Project of Shanghai, China (Grant No. B107).

†Corresponding author. E-mail: chychen@fudan.edu.cn

© 2015 Chinese Physical Society and IOP Publishing Ltd

fects. For most excitations, the two sets Υ values from both approaches agree with each other within 20%, though the importance of close-coupling effects has truly been found for a number of weak excitations, especially for those weak two-electron transitions from $3s3p^4$ to $3s^23p^23d$ configuration. The FAC code[27,29] is used throughout the present study.

2. Calculations

The present calculations are similar to our recent paper (see Wang *et al.*,[22]) which is preferred for detail calculations. Here we only present a brief description of the calculation. In the DRM calculation, we take into account the 41 levels from the $n = 3$ configurations of Cu XV in both the target CI expansion and the close-coupling expansion of the following calculation of the scattering problem. The $\boldsymbol{R}$-matrix boundary r_0 is set to enclose the 1s, 2s, 2p, 3s, 3p, and 3d orbital wavefunctions with amplitude more than 10^{-6}. Exchange effects are included for $l \leq 12$ in the $\boldsymbol{R}$-matrix inner region (i.e., $r \leq r_0$), whereas we neglect them in the outer region. To obtain detailed resonance structures, we use a 0.01 eV energy mesh for energies less than 95 eV, which is a little higher than the largest threshold of the 41 target levels as listed in Table 1, whereas a coarse energy mesh (5 eV) is used for high-energy (up to 1.5 keV) collision strength (Ω) calculations. Up to $l = 60$ partial waves and 50 radial basis functions per partial wave are considered in the calculation. Convergent Ω values with energies less than 1.5 keV are expected from these partial waves for forbidden excitations, whereas for dipole-allowed transitions, the present DRM Υ values are convergent at up to $\sim 10^{6.8}$ K from comparison with the following DW results.

In the IPIRDW approach, we calculate direct excitation (DE) and resonance excitation (RE) separately. Using the RDW method, which is also implemented in the FAC code,[27] we can straightforwardly perform the calculation of DE collision strengths. Here we take into account up to $l = 75$ of the partial-wave expansion to obtain convergent collision

Table 1. Target state energies relative to the ground state (in eV) and lifetimes of Cu XV.

No.	Conf.	Level	E(FAC)	E(NISTv5)	τ/s	LS mixing purity(No.)
1	$3s^23p^3$	$^4S_{3/2}$	0.0000	0.0000	—	94(1)
2	$3s^23p^3$	$^2D_{3/2}$	6.7081	5.9438	3.20×10^{-3}	84(2)
3	$3s^23p^3$	$^2D_{5/2}$	7.8596	7.1667	4.06×10^{-2}	100(3)
4	$3s^23p^3$	$^2P_{1/2}$	12.7378	11.2957	8.43×10^{-4}	100(4)
5	$3s^23p^3$	$^2P_{3/2}$	14.4911	13.1376	3.47×10^{-4}	81(5)
6	$3s3p^4$	$^4P_{5/2}$	40.4087	41.7950	3.97×10^{-10}	88(6)
7	$3s3p^4$	$^4P_{3/2}$	42.5747		3.52×10^{-10}	88(7)
8	$3s3p^4$	$^4P_{1/2}$	43.4422		3.26×10^{-10}	86(8)
9	$3s3p^4$	$^2D_{3/2}$	51.4934		1.70×10^{-10}	73(9)
10	$3s3p^4$	$^2D_{5/2}$	52.0556		1.98×10^{-10}	75(10)
11	$3s3p^4$	$^2P_{3/2}$	59.0868	59.2400	8.30×10^{-11}	50(26),40(11)
12	$3s3p^4$	$^2P_{1/2}$	59.7376		7.03×10^{-11}	34(13),27(35),26(12)
13	$3s3p^4$	$^2S_{1/2}$	63.0531		9.86×10^{-11}	43(13),25(35),15(12)
14	$3s^23p^2(^3P)3d$	$^4F_{3/2}$	63.1963		1.68×10^{-9}	94(14)
15	$3s^23p^2(^3P)3d$	$^4F_{5/2}$	64.0759		2.96×10^{-9}	90(15)
16	$3s^23p^2(^3P)3d$	$^4F_{7/2}$	65.3739		1.56×10^{-8}	94(16)
17	$3s^23p^2(^1D)3d$	$^2F_{5/2}$	66.3868		2.90×10^{-9}	44(17),31(36)
18	$3s^23p^2(^3P)3d$	$^4F_{9/2}$	66.8771		5.32×10^{-3}	96(18)
19	$3s^23p^2(^1D)3d$	$^2F_{7/2}$	67.3219		1.45×10^{-8}	46(23),32(19)
20	$3s^23p^2(^3P)3d$	$^4D_{1/2}$	67.3343		5.14×10^{-10}	96(20)
21	$3s^23p^2(^3P)3d$	$^4D_{3/2}$	67.5193		5.46×10^{-10}	94(21)
22	$3s^23p^2(^3P)3d$	$^4D_{5/2}$	68.5379		7.35×10^{-10}	68(22),12(17)
23	$3s^23p^2(^3P)3d$	$^4D_{7/2}$	70.7093		7.18×10^{-8}	47(23),26(19)
24	$3s^23p^2(^1D)3d$	$^2G_{7/2}$	74.8482		1.25×10^{-9}	94(24)
25	$3s^23p^2(^1D)3d$	$^2G_{9/2}$	75.6415		1.09×10^{-3}	96(25)
26	$3s^23p^2(^3P)3d$	$^2P_{3/2}$	77.9613		8.69×10^{-12}	38(11),32(37)
27	$3s^23p^2(^3P)3d$	$^4P_{5/2}$	78.2897	76.8271	6.87×10^{-12}	84(27)
28	$3s^23p^2(^3P)3d$	$^4P_{3/2}$	79.0004	77.6468	8.52×10^{-12}	59(28),14(30)
29	$3s^23p^2(^3P)3d$	$^4P_{1/2}$	79.4514	78.5190	7.14×10^{-12}	64(29),16(31)
30	$3s^23p^2(^1S)3d$	$^2D_{3/2}$	80.1836		1.64×10^{-11}	29(30),28(41),24(28)
31	$3s^23p^2(^1D)3d$	$^2P_{1/2}$	80.7794		7.93×10^{-12}	37(31),27(12),22(29)
32	$3s^23p^2(^1S)3d$	$^2D_{5/2}$	82.6060	83.7700	2.06×10^{-11}	46(40),39(32)
33	$3s^23p^2(^1D)3d$	$^2D_{5/2}$	85.8046		1.08×10^{-11}	62(33),23(32)
34	$3s^23p^2(^1D)3d$	$^2D_{3/2}$	85.8750	83.3645	7.12×10^{-12}	72(34)
35	$3s^23p^2(^3P)3d$	$^2P_{1/2}$	87.3340		7.33×10^{-12}	40(31),30(35)
36	$3s^23p^2(^3P)3d$	$^2F_{5/2}$	88.3914		5.52×10^{-12}	44(36),33(17)
37	$3s^23p^2(^1D)3d$	$^2P_{3/2}$	88.9915	87.2319	7.56×10^{-12}	46(37),29(26)
38	$3s^23p^2(^3P)3d$	$^2F_{7/2}$	89.4626	87.3105	5.63×10^{-12}	62(38),36(19)
39	$3s^23p^2(^1D)3d$	$^2S_{1/2}$	90.8064		7.55×10^{-12}	70(39)
40	$3s^23p^2(^3P)3d$	$^2D_{5/2}$	93.7658	91.1425	6.26×10^{-12}	43(40),27(32)
41	$3s^23p^2(^3P)3d$	$^2D_{3/2}$	93.8331	91.2076	6.55×10^{-12}	54(41),42(30)

strengths. Partial waves with higher contributions are considered via the Coulomb–Bethe approach. We calculate collision strengths at six scattered electron energies $E_f = 3$, 17, 104, 279, 975, and 2621 eV, during which CIs within all the 41 levels are included in the calculation.

The RE contributions are considered via the IPIRDW approach. For more details of the IPIRDW approach, our recent works on H-like Fe XXVI,[30] Ne-like Se XXV,[31] and Ni-like ions[32–35] are preferred. Here the related S-like doubly excited levels from $3s^23p^3n'l'$, $3s3p^4n'l'$, and $3s^23p^23dn'l'$ with $l' \leq 8$ are explicitly included up to $n' = 75$, and higher n' contributions up to $n' = 200$ are included via the $(n')^{-3}$ scaling law.[32,36] CI among the $3s^23p^3$, $3s3p^4$, $3s^23p^23d$ configurations are all included for Cu XV, and the CI within the same complex is considered for S-like Cu XIV. Our test calculation shows that radiative damping effects are not important (the effects are less than 2% for 99% excitations at $10^{6.4}$ K, where the fractional abundance of Cu XV peaks[37]), thus we neglect them in both DRM and IPIRDW calculations.

3. Results

In Table 1, level designations, energies, and lifetimes of the 41 levels of Cu XV are listed. The present target energies agree with the NIST ones (http://www.nist.gov/pml/data/asd.cfm) within 2 eV, but with four exceptions up to 2.6 eV for levels 34, 38, 40, and 41. We also note that, although the designation and the corresponding configuration is unique for most levels in Table 1, there exist a few levels for which the designation is ambiguous because the mixing between two levels (or even among more levels in some cases) is very strong, such as levels 12, 26, and 30. In such cases, our LS mixing purity listed in Table 1 could be helpful for further redesignation of them.

In Table 2, we report the Υ values for all the 820 excitations among the 41 levels in the temperature range of $10^{5.2} \leq T_e \leq 10^{6.8}$ K. Three sets of Υ values are reported for each excitation. The first row is the DE Υ values from the RDW calculation, the second row is the DE+RE Υ values from the IPIRDW approach (hereafter the IPIRDW ones), and the third row is the Υ values from the DRM calculation (hereafter the DRM ones). Table 2 shows that RE enlarges dramatically many excitations, and that both the IPIRDW and DRM Υ values agree well with each other for most excitations. In the following, we first make detailed comparisons between both the DRM and IPIRDW Υ values for a few typical excitations; secondly, we study the overall resonance enhancement of the Υ values and the overall agreement of Υ values from the DRM

Table 2. Effective collision strengths of excitations for Cu XV. Three sets effective collision strengths for each transition are present in this table, the first row is the DE effective collision strengths from RDW, the second and the third row are the DE+RE ones from the IPIRDW and DRM approaches. Only a portion of excitation data among the ground configuration are shown here. The whole excitation data among the 41 levels will be available in the journal homepage.

i	j	Electron temperature ($\lg T_e$, K)								
		5.2	5.4	5.6	5.8	6.0	6.2	6.4	6.6	6.8
1	2	5.40×10^{-2}	5.29×10^{-2}	5.13×10^{-2}	4.91×10^{-2}	4.63×10^{-2}	4.28×10^{-2}	3.88×10^{-2}	3.46×10^{-2}	3.04×10^{-2}
		6.34×10^{-1}	6.63×10^{-1}	6.33×10^{-1}	5.48×10^{-1}	4.36×10^{-1}	3.27×10^{-1}	2.36×10^{-1}	1.67×10^{-1}	1.17×10^{-1}
		6.39×10^{-1}	6.51×10^{-1}	6.13×10^{-1}	5.26×10^{-1}	4.17×10^{-1}	3.12×10^{-1}	2.25×10^{-1}	1.59×10^{-1}	1.12×10^{-1}
1	3	8.03×10^{-2}	7.89×10^{-2}	7.69×10^{-2}	7.41×10^{-2}	7.05×10^{-2}	6.61×10^{-2}	6.10×10^{-2}	5.56×10^{-2}	5.02×10^{-2}
		8.17×10^{-1}	7.94×10^{-1}	7.23×10^{-1}	6.10×10^{-1}	4.80×10^{-1}	3.61×10^{-1}	2.63×10^{-1}	1.91×10^{-1}	1.39×10^{-1}
		7.74×10^{-1}	7.59×10^{-1}	6.97×10^{-1}	5.90×10^{-1}	4.66×10^{-1}	3.51×10^{-1}	2.57×10^{-1}	1.86×10^{-1}	1.35×10^{-1}
1	4	1.03×10^{-2}	1.00×10^{-2}	9.59×10^{-3}	9.03×10^{-3}	8.31×10^{-3}	7.47×10^{-3}	6.54×10^{-3}	5.60×10^{-3}	4.71×10^{-3}
		1.57×10^{-1}	1.46×10^{-1}	1.26×10^{-1}	1.02×10^{-1}	7.70×10^{-2}	5.59×10^{-2}	3.94×10^{-2}	2.73×10^{-2}	1.88×10^{-2}
		1.75×10^{-1}	1.68×10^{-1}	1.50×10^{-1}	1.23×10^{-1}	9.37×10^{-2}	6.81×10^{-2}	4.78×10^{-2}	3.30×10^{-2}	2.25×10^{-2}
1	5	1.45×10^{-2}	1.40×10^{-2}	1.34×10^{-2}	1.25×10^{-2}	1.13×10^{-2}	9.99×10^{-3}	8.49×10^{-3}	6.95×10^{-3}	5.47×10^{-3}
		3.37×10^{-1}	3.22×10^{-1}	2.84×10^{-1}	2.32×10^{-1}	1.76×10^{-1}	1.27×10^{-1}	8.83×10^{-2}	5.99×10^{-2}	4.00×10^{-2}
		3.61×10^{-1}	3.56×10^{-1}	3.22×10^{-1}	2.66×10^{-1}	2.04×10^{-1}	1.47×10^{-1}	1.02×10^{-1}	6.94×10^{-2}	4.62×10^{-2}
2	3	1.57×10^{-1}	1.54×10^{-1}	1.51×10^{-1}	1.47×10^{-1}	1.41×10^{-1}	1.35×10^{-1}	1.28×10^{-1}	1.20×10^{-1}	1.13×10^{-1}
		3.35×10^{0}	2.99×10^{0}	2.58×10^{0}	2.10×10^{0}	1.62×10^{0}	1.19×10^{0}	8.52×10^{-1}	6.03×10^{-1}	4.29×10^{-1}
		2.88×10^{0}	2.57×10^{0}	2.22×10^{0}	1.82×10^{0}	1.40×10^{0}	1.04×10^{0}	7.45×10^{-1}	5.30×10^{-1}	3.79×10^{-1}
2	4	2.34×10^{-1}	2.33×10^{-1}	2.32×10^{-1}	2.30×10^{-1}	2.29×10^{-1}	2.27×10^{-1}	2.25×10^{-1}	2.24×10^{-1}	2.24×10^{-1}
		7.97×10^{-1}	7.52×10^{-1}	6.82×10^{-1}	5.92×10^{-1}	4.99×10^{-1}	4.19×10^{-1}	3.56×10^{-1}	3.11×10^{-1}	2.80×10^{-1}
		7.09×10^{-1}	6.76×10^{-1}	6.19×10^{-1}	5.42×10^{-1}	4.60×10^{-1}	3.87×10^{-1}	3.30×10^{-1}	2.89×10^{-1}	2.59×10^{-1}
2	5	1.43×10^{-1}	1.42×10^{-1}	1.41×10^{-1}	1.40×10^{-1}	1.38×10^{-1}	1.36×10^{-1}	1.33×10^{-1}	1.31×10^{-1}	1.30×10^{-1}
		7.74×10^{-1}	7.46×10^{-1}	6.80×10^{-1}	5.82×10^{-1}	4.74×10^{-1}	3.76×10^{-1}	2.98×10^{-1}	2.41×10^{-1}	2.01×10^{-1}
		7.23×10^{-1}	7.04×10^{-1}	6.50×10^{-1}	5.62×10^{-1}	4.60×10^{-1}	3.66×10^{-1}	2.89×10^{-1}	2.33×10^{-1}	1.93×10^{-1}
3	4	1.92×10^{-1}	1.91×10^{-1}	1.89×10^{-1}	1.88×10^{-1}	1.86×10^{-1}	1.84×10^{-1}	1.82×10^{-1}	1.81×10^{-1}	1.80×10^{-1}
		9.35×10^{-1}	7.74×10^{-1}	6.39×10^{-1}	5.21×10^{-1}	4.22×10^{-1}	3.46×10^{-1}	2.90×10^{-1}	2.52×10^{-1}	2.26×10^{-1}
		7.73×10^{-1}	6.67×10^{-1}	5.71×10^{-1}	4.78×10^{-1}	3.95×10^{-1}	3.26×10^{-1}	2.74×10^{-1}	2.38×10^{-1}	2.11×10^{-1}
3	5	5.35×10^{-1}	5.33×10^{-1}	5.30×10^{-1}	5.26×10^{-1}	5.22×10^{-1}	5.17×10^{-1}	5.13×10^{-1}	5.10×10^{-1}	5.08×10^{-1}
		2.04×10^{0}	1.85×10^{0}	1.63×10^{0}	1.39×10^{0}	1.16×10^{0}	9.63×10^{-1}	8.15×10^{-1}	7.09×10^{-1}	6.38×10^{-1}
		1.77×10^{0}	1.65×10^{0}	1.49×10^{0}	1.28×10^{0}	1.08×10^{0}	9.01×10^{-1}	7.64×10^{-1}	6.65×10^{-1}	5.94×10^{-1}
4	5	6.91×10^{-2}	6.81×10^{-2}	6.68×10^{-2}	6.51×10^{-2}	6.30×10^{-2}	6.04×10^{-2}	5.76×10^{-2}	5.48×10^{-2}	5.20×10^{-2}
		2.70×10^{0}	2.37×10^{0}	2.02×10^{0}	1.63×10^{0}	1.24×10^{0}	8.94×10^{-1}	6.28×10^{-1}	4.33×10^{-1}	2.99×10^{-1}
		2.09×10^{0}	1.85×10^{0}	1.59×10^{0}	1.30×10^{0}	9.92×10^{-1}	7.23×10^{-1}	5.11×10^{-1}	3.56×10^{-1}	2.48×10^{-1}

and IPIRDW approaches for all the 820 excitations; and finally, using the collisional radiative model (CRM), we calculate the line intensity ratios (or line pairs), which shows that the resonance enhancement effect is important and that the IPIRDW ones agree with those of DRM.

In Fig. 1(a), we compare cross sections and the corresponding effective collision strengths calculated by both DRM and IPIRDW approach for excitation 1–2 ($3s^23p^3\,^4S_{3/2}$–$3s^23p^3\,^2D_{3/2}$). We convolute the cross sections with a 2.35-eV normal distribution function in Fig. 1 and other following cross sections. Under such convolution, it is easier to see the resonance structures, and different Rydberg series peaks still can be separated, as shown in Fig. 1. Excitation 1–2 is a mixed (E2+M1) forbidden transition. The cross sections are dramatically enlarged in the threshold region, and the Υ values are enlarged by a factor of 10.4–2.5 over $10^{5.0}$–$10^{7.2}$ K. Both the IPIRDW and DRM background (DE) cross sections agree well with each other. Almost identical resonance structures have been obtained from both the IPIRDW and DRM approaches, while the Υ values from the two approaches also agree well with each other to within 8%. Figure 1(b) shows that the resonance contributions mainly come from the S-like $3s^23p^23dn'l'$ complex series over the whole threshold region, and the cross section peaks around 8, 25, 38, 47, and 53 eV are from the complex series with $n' = 6$–10, respectively. For other excitations among the ground configuration, there are similarly good agreements between the IPIRDW and DRM results, while the RE contributions are also dominated by the $3s^23p^23dn'l'$ complex series.

Figure 2(a) presents the Υ values of resonance transitions ($\Delta S = 0$, $\Delta L \leq 1$, E1) from the ground level to $3s3p^4$ configuration, i.e., 1–6, 7, 8 ($3s^23p^3\,^4S_{3/2}$–$3s3p^4\,^4P_{5/2,3/2,1/2}$). Resonance contributions to these strong transitions are small (less than 10%). The Υ values from both IPIRDW and DRM approaches agree with each other within 6% below $10^{6.6}$ K, and the DRM ones at higher temperature are not converged due to the high partial-waves contributions and the higher energy (above 1.5 keV) collision strengths have not been considered. Transitions from the ground level to the other 5 levels (Nos. 9–13) in the $3s3p^4$ configuration are all intercombination (spin-changed) E1 transitions. We plot the cross sections of

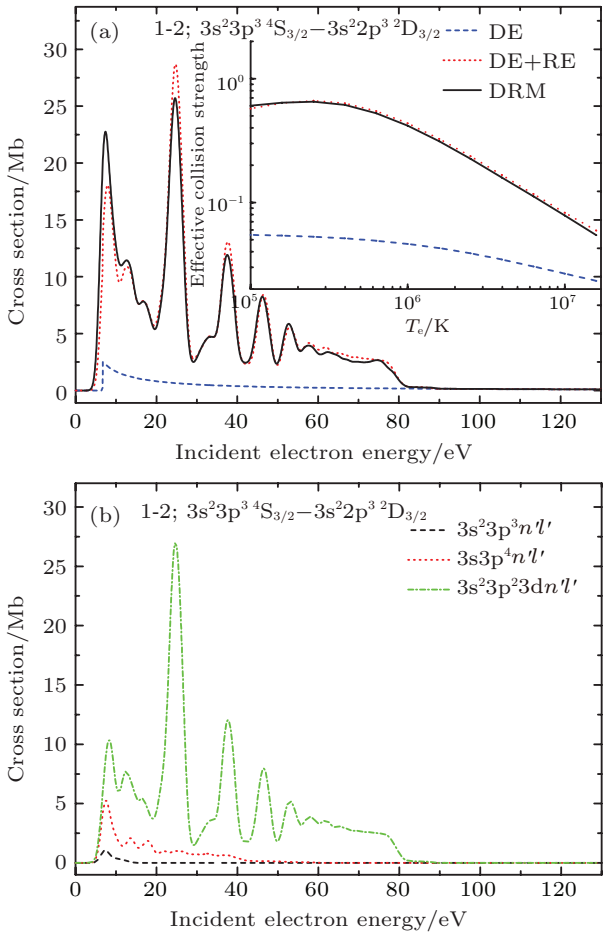


Fig. 1. (color online) Cross sections (in Mb, 1 Mb = 10^{-18} cm^2) for transitions 1–2. In panel (a), the dashed lines and the dotted lines are DE values and DE+RE values from the IPIRDW approach. The solid line is the result from DRM. The inset presents the effective collision strengths for 1–2 excitation. (b) The partial RE cross sections through $3s^23p^3n'l'$ (dashed line), $3s3p^4n'l'$ (dotted line) and $3s^23p^23dn'l'$ (dash-dot-dotted line) resonance complexes series.

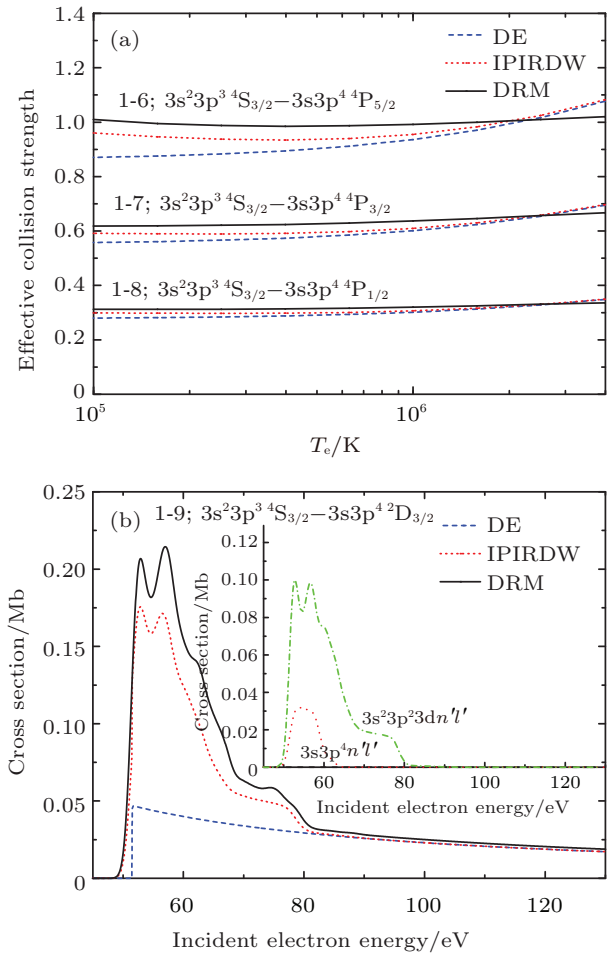


Fig. 2. (color online) (a) DE+RE effective collision strengths from both the IPIRDW and DRM approaches and DE ones from RDW for excitations 1–6, 7, and 8. (b) Cross sections from the IPIRDW and DRM approaches for excitation 1–9. The partial contributions through $3s3p^4n'l'$, and $3s^23p^23dn'l'$ resonance complexes series are shown in the inset.

excitation 1–9 ($3s^23p^3\,^4S_{3/2}$–$3s3p^4\,^2D_{3/2}$) in Fig. 2(b), and the excitation is not strong and dramatically enlarged by resonances over the threshold region. These intercombination E1 excitations are much like forbidden ones. Both the IPIRDW and DRM background cross sections agree well with each other. The IPIRDW approach underestimates the resonance contributions to these excitations. Figure 2(b) also shows that the resonance contributions mainly come from the S-like $3s^23p^23dn'l'$ complex series over the threshold region. The complex series can decay to the levels of the P-like $3s3p^4$ configuration via a three-electron transition, during which one of the three electrons is autoionized, and the orbitals of the other two electrons are changed. These three-electron transitions can occur owing to strong core mixing between $3s3p^4$ and $3s^23p^23d$ configurations. As we only consider CI within the same complex in the IPIRDW approach, the discrepancies of cross sections from the two approaches in the threshold region are not unexpected. However, for the transition, the agreement of Υ values from both approaches is still satisfactory as shown in Table 2, for example within 23% for 1–9 over the range of $10^{5.0}$–$10^{7.2}$ K. Good agreement also exists for other transitions in the array of $3s^23p^3$–$3s3p^4$, as seen from Table 2.

In Figs. 3–5, we compare certain transitions from the ground level to the levels in the $3s^23p^23d$ configuration. Figure 3 shows the Υ values of excitations 1–27, 28 and 29, i.e., $3s^23p^3\,^4S_{3/2}$–$3s^23p^2(^3P)3d\,^4P_{5/2,3/2,1/2}$, which are also resonance E1 excitations and the strongest excitations from the ground level. Resonance contributions to the three excitations can be neglected and Υ values from the IPIRDW approach are larger than its DRM counterparts at most by about 10% over the range of $10^{5.0}$–$10^{6.8}$ K. Figure 4 shows the comparison of the IPIRDW and DRM cross sections and their Υ values for excitation from the ground level to level 14 ($3s^23p^2(^3P)3d\,^4F_{3/2}$), which is a spin-unchanged and E1 transition. However, it behaves as a forbidden transition due to $\Delta L \geq 2$. The resonance enhancement of the transition is of importance at low temperature. The background cross sections from the two approaches agree with each other within 8%, though resonance structures slightly differ from each other. Consequently, the Υ values from the two approaches agree with each other within 8%. Figure 5 shows cross sections from the two approaches and Υ values for forbidden transition 1–24, i.e., $3s^23p^3\,^4S_{3/2}$–$3s^23p^2(^1D)3d^2G_{7/2}$, which is a rather weak transition and resonance excitation dominates over all the temperature range. Resonance contributions can enhance the Υ values by up to around two orders of magnitude at low temperatures. The DRM background cross sections are larger than its IPIRDW counterparts by around 20%. The cross sections from the two approaches agree well with each other and the agreement of the corresponding Υ values are within 28%, which is still acceptable.

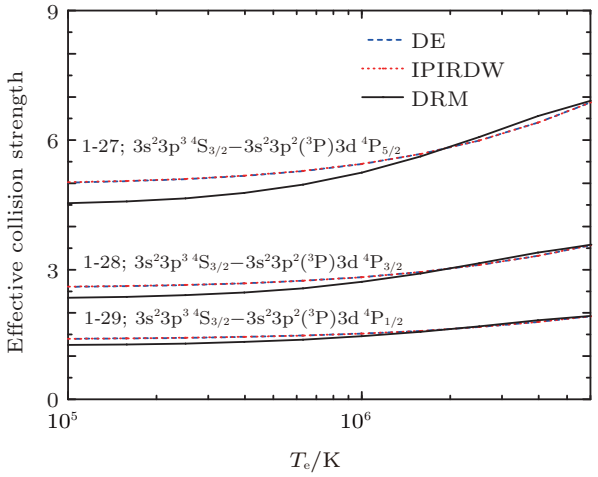


Fig. 3. (color online) DE+RE effective collision strengths from both the IPIRDW and DRM approaches and DE ones from RDW for excitations 1–27, 28, and 29.

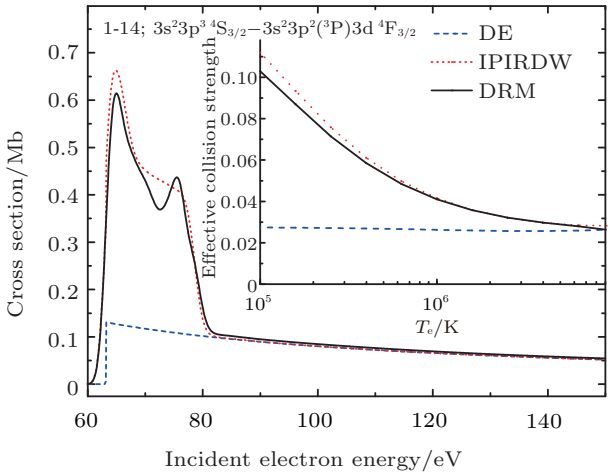


Fig. 4. (color online) Cross sections (in Mb, 1 Mb = 10^{-18} cm^2) from the IPIRDW and DRM approaches and DE background ones for excitation 1–14, of which the effective collision strengths are shown in the inset.

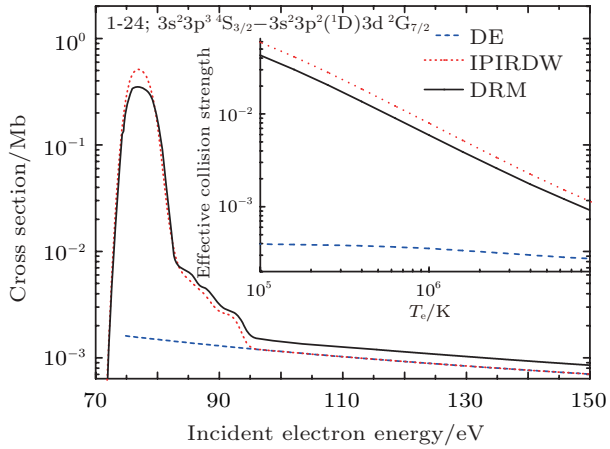


Fig. 5. (color online) Cross sections and effective collision strengths for excitation 1–24, the same as Fig. 4.

Figures 6 and 7 show the comparisons of two rather weak (as indicated from their cross sections) two-electron-transition excitations 7–24 and 6–27 between the levels of $3s3p^4$ and $3s^23p^23d$ configurations. Such excitations can occur because

of the interaction between these two configurations. For most two-electron-transition excitations, the Υ values from the two approaches agree well with each other. As shown in Fig. 6 for 7–24 excitation, the agreement of the Υ values from the two approaches is satisfactory, being within 16% over the range of $10^{5.0}$–$10^{7.0}$ K, and resonance enhancements of the excitation over the threshold region are of vital importance. However, for a number of two-electron-transition excitations, the Υ values from the two approaches largely differ from each other, which shows the importance of the close-coupling effects. As shown in Fig. 7 for 6–27 excitation, the close-coupling effects are so important for the excitation that the DRM Υ values are larger than their IPIRDW counterparts by up to a factor of about 2, whereas the resonance enhancements of the excitation are so small that they could be neglected.

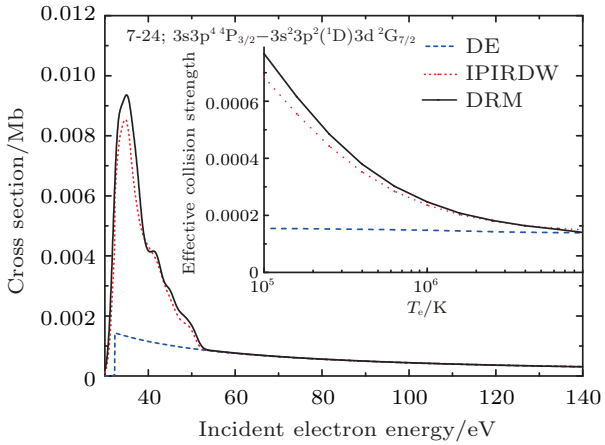


Fig. 6. (color online) Cross sections and effective collision strengths for a two-electron excitation 7–24, the same as Fig. 4.

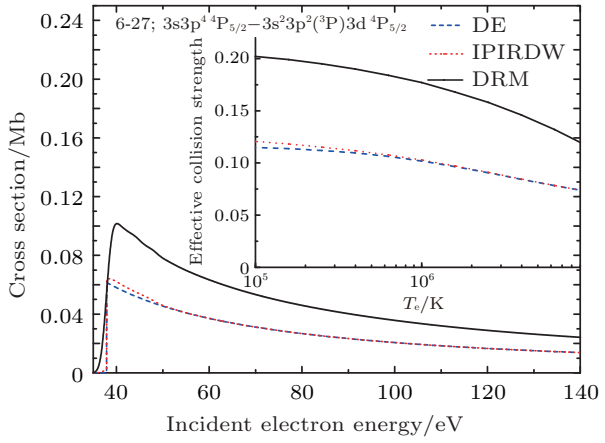


Fig. 7. (color online) Cross sections and effective collision strengths for a two-electron excitation 6–27, the same as Fig. 4.

Figure 8, in which we present the ratios of the DE+RE Υ values to the DE ones at $T_e = 10^{5.2}$ K, shows the overall importance of resonance contributions to Υ values. Statistic results show that resonance contributions can enlarge the Υ values at $T_e = 10^{5.2}$ K by more than 20% and a factor of 2 for 112 and 244 out of all the 820 transitions, respectively. Whereas at higher temperature, resonance contributions become smaller as expected.

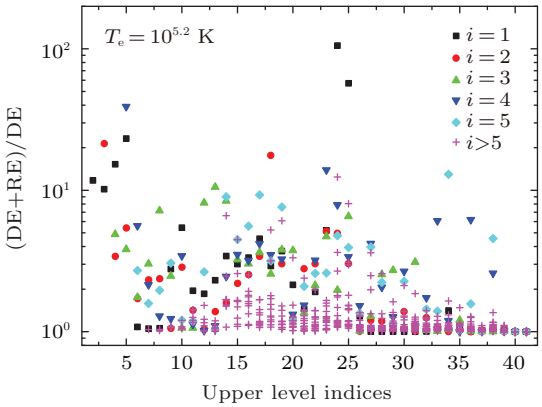


Fig. 8. (color online) DE+RE effective collision strengths from the IPIRDW approach over the DE ones from the RDW method at $T_e = 10^{5.2}$ K. The horizontal axis values are the upper level of excitations. The squares, circles, up-triangles, down-triangles, diamonds, and crosses are the excitations from levels $i = 1$, 2, 3, 4, 5, and others, respectively.

Figure 9 shows the overall comparison of Υ values from the two approaches at $T_e = 10^{6.4}$ K, where the fractional abundance is of Cu XV peaks.[37] Statistic results show that the Υ values from the two approaches agree with each other within 20% for 670 out of all the 820 transitions. There are 112 excitations with large difference (more than 20%) between the two sets of Υ values, for which the DRM ones are all larger than the IPIRDW one. In addition, most of the excitations (67 out of 112 transitions) are the two-electron transitions from the $3s3p^4$ to $3s^23p^23d$ configuration. The large differences obviously come from the differences between the background collision strengths from the two approaches.

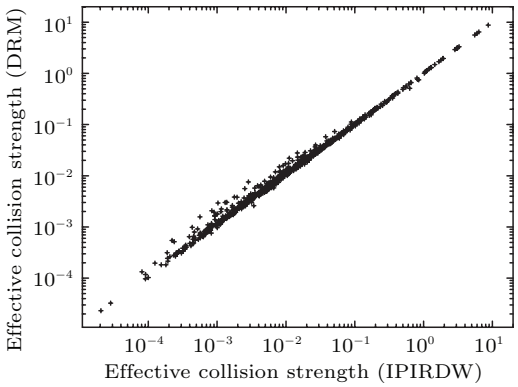


Fig. 9. Comparisons of effective collision strengths from the IPIRDW and DRM approaches at $T_e = 10^{6.4}$ K.

P-like ions are very useful for density diagnostics.[2,19,26] The most useful density diagnostics line pairs (or line intensity ratios) are related to the strong allowed lines from the $3s^23p^3$ to $3s^23p^23d$ configuration with wavelengths in the range of

132–255 Å, and those from the $3s^23p^3$ to $3s3p^4$ configuration with wavelengths in the range of 196–479 Å. To illustrate the resonance excitation effects on line pairs, we make a test calculation using the collisional radiative model (CRM), in which electron impact excitation and de-excitation rates, radiative rates among the 41 levels are considered. All the E1, M1, E2, and M2 radiative rates are calculated by using the FAC code. Employing the electron impact excitation data in Table 2 together with steady-state rate equations from Dufton,[38] we can obtain relative level populations and subsequently emission-line intensities of Cu XV. Present results show that resonance contributions significantly change the relative level populations and dramatically influence the density diagnostics line pairs. Figure 10 presents two line intensity ratios or line pairs (in photon units) over the density range of $10^{8.8}$–$10^{12.2}$ cm^{-3} at $10^{6.4}$ K. We note that the two line pairs have been used for density diagnostics in the case of P-like Fe XII.[2] Resonance contributions enlarge significantly the ratios by 26%–37% at the density below $10^{9.4}$ cm^{-3}. It also shows that the line intensity ratios from the DRM and IPIRDW approaches agree well with each other, though large differences between the two sets of Υ values exist for some weak transitions, especially for two-electron excitations as we mentioned above.

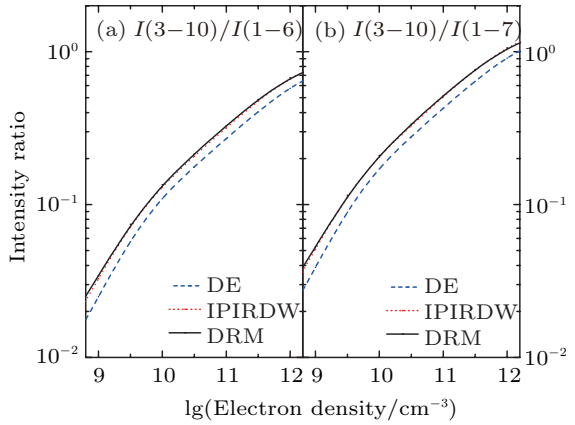


Fig. 10. (color online) (color online) Line intensity ratios (in photon units) of line pairs (a) 3–10/1–6 and (b) 3–10/1–7 at $T_e = 10^{6.4}$ K are obtained from CRM together with DE+RE effective collision strengths from the IPIRDW (dotted-line) and DRM (solid line) approaches and DE ones from the RDW method (dashed-line).

4. Conclusions

Employing both the Dirac $\boldsymbol{R}$-matrix and the relativistic distorted wave with an independent process and isolated resonance approaches, we report resonance enhanced electron impact excitation data (specifically, effective collision strengths) among the lowest 41 levels from the $n = 3$ configurations of Cu XV over $10^{5.2}$–$10^{6.8}$ K. It is found that resonance contributions dramatically (over two orders of magnitude) enlarge many excitations, and that the effective collision strengths obtained from the two approaches agree with each other for most excitations, though close-coupling effects are truly significant for weak excitations, especially for two-electron excitations. Density diagnostic line intensity ratios from the two approaches agree well with each other and are enhanced by resonance contributions by up to 37%. To the best of our knowledge, this is the first study on electron impact excitation of Cu XV.

References

[1] Träbert E, Beiersdorfer P, Brickhouse N S and Golub L 2014 *Astrophys. J. Suppl. Ser.* 215
[2] Storey P J, Del Zanna G, Mason H E and Zeippen C J 2005 *Astron. Astrophys.* **433** 717
[3] Shirai T, Sugar J, Musgrove A and WieseW L 2000 *Spectral Data for Highly Ionized Atoms: Ti, V, Cr, Mn, Fe, Co, Ni, Cu, Kr and Mo* (New York: AIP Press Melville) p. 401
[4] Chaurasia S, Munda D S, Murali C G, Gupta N K and Dhareshwar L J 2008 *J. Appl. Phys.* **103** 013307
[5] Jochen S, Ogden J, Mordecai R, Eduard D, Siegfried G, Janelle G, Bruce H, Otto L, Laurence S and Russell W 2007 *Phys. Rev. Lett.* **98** 175003
[6] Moses E I 2009 *Nucl. Fusion* **49** 104022
[7] Liu P F, Liu Y P, Zeng J L and Yuan J M 2014 *Phys. Rev. A* **89** 042704
[8] Chen Z B, Dong C Z, Xie L Y and Jiang J 2014 *Chin. Phys. Lett.* **31** 033401
[9] Fan Q P, Wang W H, Hu F, Cao L F, Zhang Q Q, Liu Y W and Jiang G 2014 *Chin. Phys. B* **23** 113401
[10] Vilkas M J and Ishikawa Y 2004 *J. Phys. B* **37** 4763
[11] Träbert E, Fritzsche S and Jupén C 1998 *Eur. Phys. J. D* **3** 13
[12] Huang K N 1984 *At. Data Nucl. Data Tables* **30** 313
[13] Tayal S S and Zatsarinny O 2010 *Astrophys. J. Suppl. Ser.* **188** 32
[14] Sossah A M and Tayal S S 2012 *Astrophys. J. Suppl. Ser.* **202** 12
[15] Wilson N J and Bell K L 2001 *Mon. Not. Roy. Astron. Soc.* **325** 159
[16] Hudson C E 2009 *Phys. Scr.* **79** 035301
[17] Binello A M, Mason H E, and Storey P J 1998 *Astron. Astrophys. Suppl.* **131** 153 9
[18] Binello A M, Mason H E, and Storey P J 1998 *Astron. Astrophys. Suppl.* **127** 545
[19] Del Zanna G and Mason H E 2005 *Astron. Astrophys.* **433** 731
[20] Del Zanna G, Storey P J, Badnell N R, and Mason H E 2012 *Astron. Astrophys.* **543** A139
[21] Landi E and Bhatia A K 2010 *At. Data Nucl. Data Tables* **96** 52
[22] Wang K, Chen C Y, Huang M, Wang Y S, Zou Y M and Zeng J L 2010 *J. Phys. B* **43** 175202
[23] Cowan R D 1980 *J. Phys. B* **13** 1471
[24] Seaton M J 1976 *Adv. At. Mol. Phys* **11** 83
[25] Burke P G and Robb W D 1976 *Adv. At. Mol. Phys* **11** 143
[26] Binello A M, Landi E, Mason H E, Storey P J and Brosius J W 2001 *Astron. Astrophys.* **370** 1071
[27] Gu M F 2008 *Can. J. Phys.* **86** 675
[28] Gu M F 2004 *Phys. Rev. A* **70** 062704
[29] Gu M F 2003 *Astrophys. J.* **582** 1241
[30] Chen C Y, Wang K, Huang M, Wang Y S and Zou Y M 2010 *J. Quant. Spect. Radiat. Trans.* **111** 843
[31] Wang K, Chen C Y, Huang M, Wang Y S and Zou Y M 2011 *At. Data Nucl. Data Tables* **97** 426
[32] Shen T M, Chen C Y, Wang Y S, Zou Y M and Gu M F 2007 *J. Phys. B* **40** 3075
[33] Shen T M, Chen C Y, Wang Y S and Zou Y M 2009 *Eur. Phys. J. D* **53** 179
[34] Shen T M, Chen C Y, Wang Y S, Zou Y M and Gu M F 2007 *Phys. Rev. A* **76** 022703
[35] Zhang Y, Chen C Y, Wang Y S and Zou Y M 2009 *J. Quant. Spect. Radiat. Trans.* **110** 2180
[36] Hahn Y 1985 *Adv. At. Mol. Phys.* **21** 123
[37] Dufton P L 1977 *Comput. Phys. Commun.* **13** 25
[38] Mazzotta P, Mazzitelli G, Colafrancesco S and Vittorio N 1998 *Astron. Astrophys. Suppl.* **133** 403